TITLE

AUTHORS[1]

ABSTRACT

ABSTRACT

Subject headings: KEYWORDS

1. Introduction

Irregularities in the ionized interstellar medium (ISM) scatter radio waves, leading to familiar effects, such as scintillation of sources. For sources that can be spatially resolved, the scattering also causes blurring and distortion of the image, analogous to the deleterious effects of the atmosphere on optical observations. Hence, as radio observations achieve ever higher angular resolution, these effects of the ISM on imaging become increasingly important considerations. In this paper, we consider the effects of interstellar scattering on resolved images of the Galactic Center supermassive black hole, Sagittarius A* (Sgr A*).

Sgr A* has been studied with very-long-baseline interferometry (VLBI) for the last 40 years. At wavelengths longer than a centimeter, the size of the image of Sgr A* grows with the squared observing wavelength. This scaling is typical when the angular broadening of a source from ISM scattering is much larger than the angular size of the source. At wavelengths shorter than a centimeter, the source angular size is larger than expected from this scaling, indicating the presence of intrinsic structure in addition to the angular broadening. The shortest-wavelength VLBI observations to-date were performed at 1.3-mm with the Event Horizon Telescope (Doeleman et al. 2008; Fish et al. 2011). At this wavelength, the angular broadening ($\sim$20 μas) is subdominant to intrinsic structure ($\sim$40 μas).

Nevertheless, features such as a bright ring surrounding the "shadow" of the black hole can still be affected by the residual scatter-broadening. Recently, Fish et al. (2014) has shown that these effects can be effectively mitigated in the ensemble-average regime, where the "blurring" of scattering is deterministic. Our goal is to use numerical simulations of the scattering to investigate the potential contribution of scattering-induced substructure for realistic images and observations.

[1]Harvard-Smithsonian Center for Astrophysics, 60 Garden Street, Cambridge, MA 02138, USA

1.1. Interstellar Scattering

The scattering of Sgr A* below about 2 THz is "strong": the electric field seen by the observer consists of the superposition of many rays from different paths, whose phase from scattering differs by many radians across the extent of the scattered image. For strong scattering, effects are divided into two distinct branches: diffractive and refractive. These branches have strikingly different properties.

Diffractive effects are narrowband, short-lived, and quenched by all but the most compact sources, such as pulsars. Refractive effects are wideband, long-lived, and only begin to be quenched when a source exceeds the size of the scattered image of a point source (i.e., when the effects of scatter-broadening become subdominant to intrinsic structure). Diffractive effects become stronger at longer wavelengths, whereas refractive effects become stronger at shorter wavelengths.

Scattering also exhibits two opposite effects depending on the degree of averaging in time. When averaged over long timescales (an ensemble-average), scattering acts to blur the image of a source. In contrast, over shorter timescales, scattering introduces substructure in the image of the source, exaggerating gradients in the unscattered image. Remarkably, the substructure can persist over long timescales, as was first shown by Narayan & Goodman (1989) and Goodman & Narayan (1989), and can be an important consideration even when the scattering is subdominant to intrinsic structure, as was shown by Johnson & Gwinn (2015, hereafter JG15).

State conditions for validity of the geometric optics approximation (recast differently, with source coordinates rather than screen?):

$$\begin{aligned} I_{\rm ss}(\mathbf{x}) &\approx \int d^2\mathbf{y}\, V_{\rm src}\left((1+M)\mathbf{y}\right) e^{-i\mathbf{y}\cdot\nabla\phi(\mathbf{x})} e^{-\frac{i}{r_{\rm F}^2}\mathbf{y}\cdot\mathbf{x}} \\ &= I_{\rm src}\left(\mathbf{x} + r_{\rm F}^2\nabla\phi(\mathbf{x})\right). \end{aligned} \tag{1}$$

Note that the action of scattering shuffles brightness elements of the source but does not conserve total flux.

need definitions In this limit, the frequency evolution of the scattering is especially simple. The Fresnel scale, $r_{\rm F}$, is proportional to $\sqrt{\lambda}$. The behavior of $\phi(\mathbf{x})$ follows from the refractive index of a dilute plasma at a frequency well above its plasma frequency, $\nu_{\rm p}$: $n \approx 1 - \frac{1}{2}\frac{\nu_{\rm p}^2}{\nu^2}$. Hence, $\phi(\mathbf{x}) \propto (n-1)/\lambda \propto \lambda$. Thus, in this regime, scattering displaces a given brightness element of the source by an amount proportional to λ^2.

Hence, we can rewrite the action of scattering as $I_{\rm ss}(\mathbf{x}) \approx I_{\rm src}\left(\mathbf{x} + \left(\frac{\lambda}{\lambda_0}\right)^2 \mathbf{s}_0(\mathbf{x})\right)$. Once the vector field $\mathbf{s}_0(\mathbf{x})$ is measured at a single wavelength λ_0 over some angular domain D, the scattering can be inverted at all frequencies over the same domain D. If the intrinsic structure is sufficiently simple so that scattering features can be identified, then one can use the comparison of scattered

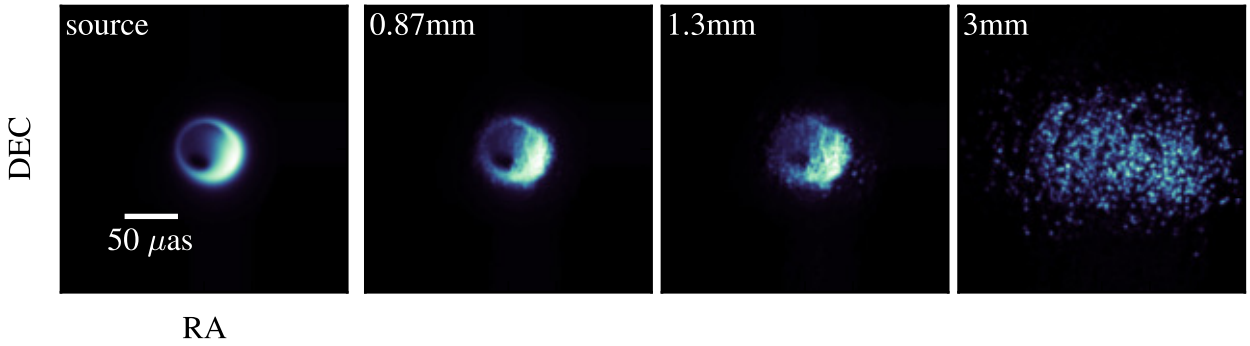

Fig. 1.— A source is shown in the left most panel and scattered instances of the same source at 0.87, 1.3, and 3 mm are displayed from left to right. All images are smoothed by a 3 μas Gaussian.

images at different wavelengths to perform relative astrometry of source components (cite quasar stuff).

A given solution at one observing wavelength can then be used to infer the scattering properties at other wavelengths. And because of the steep scaling with wavelength, the scattering can be characterized at long wavelengths, where scatter-broadening is easily measured, and then applied to shorter wavelengths, where it is difficult to resolve or degenerate with structure from the unscattered source.

2. Methods

Should define scattered versus source image. Mention code here.

3. Scattering at different wavelengths

Show realizations of scattering at 0.87, 1.3, and 3 mm.

4. Reconstruction of a scattered image

Show how Vincent's method works on these images. Does averaging really help for imaging with the bispectrum? If not, can we estimate which baselines are garbage for imaging?

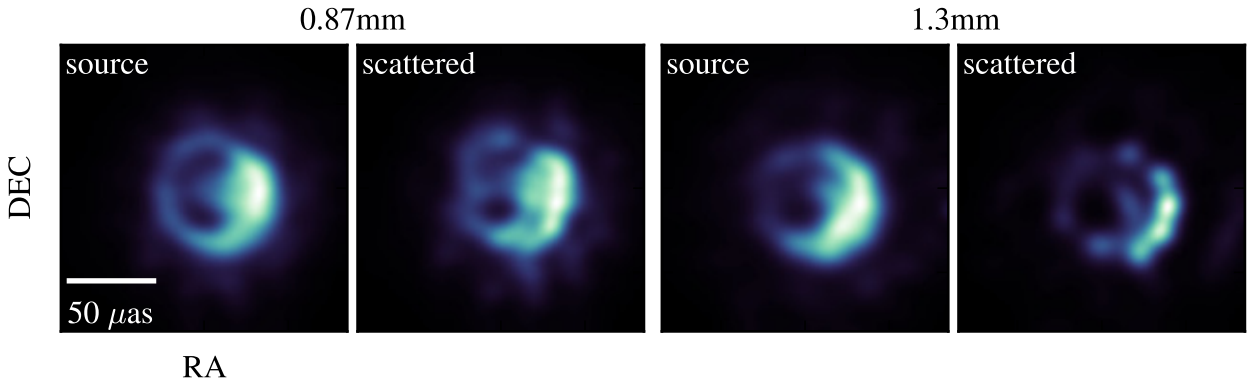

Fig. 2.— These panels show images reconstructed using the bispectrum and the maximum entropy algorithm. The original images are the same ones as shown in Figure 1. The uv-samples were set by baselines between the SMA, SMT, PV, ALMA, SPT, PDB, and LMT. All images are smoothed by a Gaussian with FWHM of 10 μas

5. Ring Size

One application of EHT observations is measuring properties of the photon ring. This phenomenon traces where photons emitted from the accretion disk wrap multiple times around the black hole, creating a brightness concentration that outlines the black hole shadow. The diameter of this ring is $3\sqrt{3}GM/c^2$ which corresponds to an angular size of 52 μas for Sgr A*($M_{\rm BH} = 4.3 \times 10^6\,M_\odot$ at a distance of 8.4 kpc). The shape of this ring is a powerful test of general relativity with its shape and ellipticity indicating a possible deviation from the Kerr metric (**??**). Consequently, it is important to properly estimate the uncertainties in the apparent ring shape due to distortion by scattering.

We consider the source to be a uniform annulus with width to diameter ratio, $a = \Delta/d$, and the diameter, d, is the arithmetic mean of the inner and outer edge of the annulus. For this simple source, the visibility amplitude is the different between two Bessel functions of the first kind:

$$|V_{\rm annulus}(\rho)| = \frac{(1+a)J_1[\pi d(1+a)\rho] - (1-a)J_1[\pi d(1-a)\rho]}{\pi d\rho}. \quad (2)$$

Equation 2 shows that for a given width to diameter ratio a, the first (or any) null can be used to determine the diameter of the annulus, d. The left panel in Figure 3 shows the position of the first null of the visibility amplitude as a function of a. Using an annulus where $d = 57$ and $\Delta = 22$ (the fit from Doeleman et al. (2008)), we generate 50 independent instances the scattered source and calculate a diameter using the position of the first null along the major and minor axis of the scattering kernel. The right panel in Figure 3 shows the resulting rms error for observations at 230 and 350 GHz. Even at 350 GHz, the 1-σ scatter is similar to the shift between a ring ($a = 0$) and

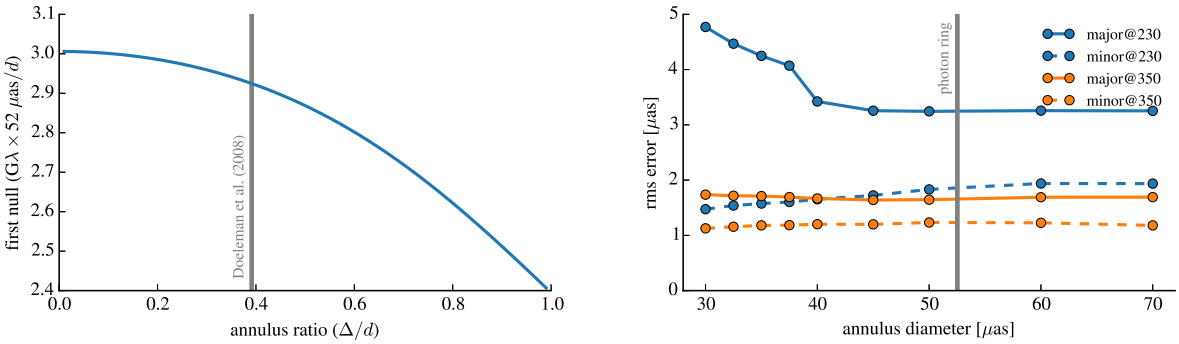

Fig. 3.— *Left*: Position of the first null for a uniform annulus as a funtion of its diameter to width ratio. The gray line indicates the annulus ratio, $a = 22/57$, from the obsevations presented by Doeleman et al. (2008). *Right*: The root mean square error introduced by scattering on the derived annulus width. Note that this effect is at least as large as the shift in the null going from a ring ($a = 0$) to a full disk ($a = 1$).

full disk ($a = 1$) source model. For large enough ring sizes, the rms error appears to be independent of the ring size. However, there is a significant increase in the rms for annulli with diameters less than $40\,\mu$as. Here the scale of the scattering blur $22\,\mu$as) is as large as the radius, filling in the inner hole and introducing a bias towards smaller diameters. For an annulus with $d = 50\,\mu$as, the mean eccentricity that would be calculed using the major and minor axis diameters is 0.3 and 0.2 at 230 and 350 GHz.

6. Uncertainty in the scattering parameters

7. Conclusion

REFERENCES

Doeleman, S. S., Weintroub, J., Rogers, A. E. E., Plambeck, R., Freund, R., Tilanus, R. P. J., Friberg, P., Ziurys, L. M., Moran, J. M., Corey, B., Young, K. H., Smythe, D. L., Titus, M., Marrone, D. P., Cappallo, R. J., Bock, D. C.-J., Bower, G. C., Chamberlin, R., Davis, G. R., Krichbaum, T. P., Lamb, J., Maness, H., Niell, A. E., Roy, A., Strittmatter, P., Werthimer, D., Whitney, A. R., & Woody, D. 2008, Nature, 455, 78

Fish, V. L., Doeleman, S. S., Beaudoin, C., Blundell, R., Bolin, D. E., Bower, G. C., Chamberlin, R., Freund, R., Friberg, P., Gurwell, M. A., Honma, M., Inoue, M., Krichbaum, T. P., Lamb, J., Marrone, D. P., Moran, J. M., Oyama, T., Plambeck, R., Primiani, R., Rogers, A. E. E., Smythe, D. L., SooHoo, J., Strittmatter, P., Tilanus, R. P. J., Titus, M., Weintroub, J., Wright, M., Woody, D., Young, K. H., & Ziurys, L. M. 2011, The Astrophysical Journal Letters, 727, L36

Fish, V. L., Johnson, M. D., Lu, R.-S., Doeleman, S. S., Bouman, K. L., Zoran, D., Freeman, W. T., Psaltis, D., Narayan, R., Pankratius, V., Broderick, A. E., Gwinn, C. R., & Vertatschitsch, L. E. 2014, The Astrophysical Journal, 795, 134

Goodman, J. & Narayan, R. 1989, Monthly Notices of the Royal Astronomical Society, 238, 995

Johnson, M. D. & Gwinn, C. R. 2015, The Astrophysical Journal, 805, 180

Narayan, R. & Goodman, J. 1989, Monthly Notices of the Royal Astronomical Society, 238, 963